

Exploring non-radial oscillation modes in dark matter admixed neutron stars

Pratik Thakur^{*a}, Anil Kumar^{†a}, Vivek Baruah Thapa^{‡b}, Vishal Parmar^{§c}, and
Monika Sinha^{¶a}

^aIndian Institute of Technology Jodhpur, , Jodhpur 342037, India

^bDepartment of Physics, Bhawanipur Anchalik College,, Barpeta, Assam
781352, India

^cINFN, Sezione di Pisa, Largo B. Pontecorvo 3, I-56127 Pisa, Italy

January 22, 2025

Abstract

Because of their extreme densities and consequently, gravitational potential, compact objects such as neutron stars can prove to be excellent captors of dark matter particles. Considering purely gravitational interactions between dark and hadronic matter, we construct dark matter admixed stars composed of two-fluid matter subject to current astrophysical constraints on maximum mass and tidal deformability. We choose a wide range of parameters to construct the dark matter equation of state, and the DDME2 parameterization for the hadronic equation of state. We then examine the effect of dark matter on the stellar structure, tidal deformability and non-radial modes considering the relativistic Cowling approximation. We find the effect on p -modes is substantial, with frequencies decreasing up to the typical f -mode frequency range for most stars with a dark matter halo. The effects on the f -mode frequency are less extreme. Finally, we find the most probable values of the dark matter parameters that satisfy the observational constraints.

^{*}thakur.16@iitj.ac.in

[†]anil.1@iitj.ac.in

[‡]thapa.1@iitj.ac.in

[§]vishalparmar@iitj.ac.in

[¶]corresponding author: ms@iitj.ac.in

1 Introduction

There are indirect pieces of evidence from cosmological and astrophysical observations such as rotation curves of individual galaxies, observed galaxy clusters, and anisotropic microwave background that the dominant contribution to the matter in the universe is in the form of “dark matter” (DM) whose cross-section with baryons is very small [1]. The search for direct detection of DM particles is also ongoing in several experiments [2–4]. A well-studied model for DM involves weakly interacting massive particles (WIMPs) with masses ranging from the GeV to the TeV scale. The upper bound of WIMPs scattering off the nuclei is estimated to be $\sim 10^{-47}$ cm² from underground direct search experiments such as CDMS [5], Xenon1T [6] and XENONnT [7]. Despite the tiny value of the scattering cross-section of DM with ordinary matter, the gravitational impact of DM is very significant. However, nearly all properties of DM remain largely unknown. If DM exists, understanding its nature would provide significant advancements in our knowledge beyond standard model physics [8].

Many cosmological problems such as the “core-cusp problem,” the “missing satellite problem”, and the “too big to fail problem” could potentially be addressed by considering the DM as self-interacting [9, 10]. Self-interacting DM particles may be self-annihilating or non-self-annihilating. If they are self-annihilating, after their capture by compact objects, they will annihilate, releasing heat inside the compact objects [11–14]. On the other hand, if they do not annihilate, these particles will accumulate within compact objects, provided the dark matter particle is a WIMP [15, 16]. Hence, the compact star with a large number of accreted DM in the core will easily exceed the Schwarzschild limit and consequently collapse. The asymmetric DM is an interesting alternative of the annihilating WIMP paradigm [17–35].

Because of the gravitational impact of DM, its properties can be constrained from its effect on the formation and evolution of stars [36, 37]. Compact objects, in this sense, are potential candidates to study DM, not only because of immense gravity which increases the possibility of the capture of DM particles, but also for their high baryonic density, which increases the probability of DM-nucleon scattering [11, 16, 38–42]. DM admixed compact stars have been explored in several previous works, considering a variety of DM and baryonic matter EOSs [43–58].

The recently found lower bound in maximum attainable mass of compact stars [59] raises questions on the appearance of heavier strange and non-strange baryons in the inner core of the baryonic stars [60]. However, the appearance of these degrees of freedom softens the matter at high density regimes which lowers the maximum attainable mass. If by altering the theoretical proposed model for this kind of matter- for example by taking density-dependent interactions among baryons [61–63], the matter becomes stiff, the maximum limit of tidal deformability can not be fulfilled [64]. However, as will be shown, the presence of DM can significantly alter the stellar structure, and both the lower limit of maximum attainable mass and the upper limit of tidal deformability can be achieved simultaneously. Consequently, the study of DM admixed compact star property which is very important from particle physics as well as from astrophysical aspects.

We have constructed the DM admixed compact star considering only the gravitational interaction of self-interacting but non-self-annihilating DM with ordinary matter as in refs. [65, 66]. Interested readers may refer to [45, 54, 67]. Due to the lack of evidence and proper knowledge of DM interaction with ordinary matter, we avoid such beyond-standard model interactions in the present work. For a compact star, we consider a neutron star (NS) to be

composed of nucleonic matter or hyperons are also present at high density. We study the effect on the NS properties connected to the recent and upcoming stellar observations considering the scenario in DM admixed NS. Further, in this context, we will discuss the properties of non-radial oscillations for such stars.

There are several quasi-normal modes like the fundamental (f)-mode, pressure (p)-modes, gravity (g)-modes, spacetime (w)-mode, etc [68–70], each classified based on the restoring forces which work bring the star to equilibrium. For example, the f - and p_1 - (with only one radial node in fluid perturbation amplitude) modes, which are acoustic waves in the star, are restored by fluid pressure while g -modes which arise due to density discontinuities or temperature and composition variations are restored by gravity (buoyancy). Several of these modes can be excited during a supernova explosion or in a remnant of a binary merger [71–73]. Even during the inspiral phase of compact stars, the f -mode may be excited [74]. Quadrupolar oscillations ($l = 2$) of all modes couple to gravitational waves. With the advent of enhanced next-generation telescopes like the Cosmic Explorer and the Einstein telescope which carry about 10 times the sensitivity of Advanced LIGO, the possibility of detection of these modes increases [71].

2 Hadronic matter model

The model for hadronic matter (HM) we discussed here, we assume that normal matter is composed of protons, neutrons, hyperons (Λ , Σ and Ξ), and electrons. We consider the relativistic mean field model for ordinary HM where the interaction between these baryons is carried by isoscalar-scalar σ , isoscalar-vector ω , and isovector-vector ρ mesons along with density-dependent interaction. Additionally, the interaction between hyperons is mediated through isoscalar-scalar σ^* and isoscalar-vector ϕ meson. The Lagrangian density for HM is given as [75]

$$\begin{aligned} \mathcal{L}_{HM} = & \sum_b \bar{\psi}_b (i\gamma_\mu D^\mu - m_b^*) \psi_b + \frac{1}{2} (\partial_\mu \sigma \partial^\mu \sigma - m_\sigma^2 \sigma^2) + \frac{1}{2} (\partial_\mu \sigma^* \partial^\mu \sigma^* - m_{\sigma^*}^2 \sigma^{*2}) \\ & - \frac{1}{4} \omega_{\mu\nu} \omega^{\mu\nu} + \frac{1}{2} m_\omega^2 \omega_\mu \omega^\mu - \frac{1}{4} \phi_{\mu\nu} \phi^{\mu\nu} + \frac{1}{2} m_\phi^2 \phi_\mu \phi^\mu - \frac{1}{4} \rho_{\mu\nu} \cdot \rho^{\mu\nu} + \frac{1}{2} m_\rho^2 \rho_\mu \cdot \rho^\mu \end{aligned} \quad (1)$$

Here b denotes baryons, and covariant derivative $D_\mu = \partial_\mu + ig_{\omega b} \omega_\mu + ig_{\phi b} \phi_\mu + ig_{\rho N} \tau_{N3} \cdot \rho_\mu$. ψ_b is the baryonic wavefunction, σ the σ -meson, σ^* the σ^* -meson, ω_μ the ω -meson, ϕ_μ the ϕ -meson and ρ_μ the ρ -meson fields. The effective baryon mass is $m_b^* = m_b - g_{\sigma b} \sigma - g_{\sigma^* b} \sigma^*$. The antisymmetric field terms due to vector meson fields are given by $\omega_{\mu\nu} = \partial_\mu \omega_\nu - \partial_\nu \omega_\mu$, $\phi_{\mu\nu} = \partial_\mu \phi_\nu - \partial_\nu \phi_\mu$ and $\rho_{\mu\nu} = \partial_\mu \rho_\nu - \partial_\nu \rho_\mu$. The isoscalar meson-baryon couplings vary with density as

$$g_{ib}(n) = g_{ib}(n_0) f_i(x) \quad \text{for } i = \sigma, \sigma^*, \omega, \phi \quad (2)$$

where the function is given by

$$f_i(x) = a_i \frac{1 + b_i(x + d_i)^2}{1 + c_i(x + d_i)^2} \quad (3)$$

with $x = n/n_0$ and a_i , b_i , c_i , d_i the parameters that describe the density-dependent nature of the coupling parameters. The isovector-vector ρ -meson coupling with baryons is given by $g_{\rho b}(n) = g_{\rho b}(n_0) e^{-a_\rho(x-1)}$.

With this model, the energy density ε and pressure p of hadronic matter are given by

$$\begin{aligned} \varepsilon_{HM} = & \frac{1}{2}m_\sigma^2\sigma^2 + \frac{1}{2}m_{\sigma^*}^2\sigma^{*2} + \frac{1}{2}m_\omega^2\omega_0^2 + \frac{1}{2}m_\phi^2\phi_0^2 + \frac{1}{2}m_\rho^2\rho_{03}^2 + \frac{1}{4\pi^2} \sum_b \left[p_{F_b} E_{F_b}^3 - \frac{m_b^{*2}}{2} \left(p_{F_b} E_{F_b} \right. \right. \\ & \left. \left. + m_b^{*2} \ln \left(\frac{p_{F_b} + E_{F_b}}{m_b^*} \right) \right) \right] + \frac{1}{4\pi^2} \sum_l \left[p_{F_l} E_{F_l}^3 - \frac{m_l^2}{2} \left(p_{F_l} E_{F_l} + m_l^2 \ln \left(\frac{p_{F_l} + E_{F_l}}{m_l} \right) \right) \right] \end{aligned} \quad (4)$$

and,

$$\begin{aligned} p_{HM} = & -\frac{1}{2}m_\sigma^2\sigma^2 + \frac{1}{2}m_{\sigma^*}^2\sigma^{*2} + \frac{1}{2}m_\omega^2\omega_0^2 + \frac{1}{2}m_\phi^2\phi_0^2 + \frac{1}{2}m_\rho^2\rho_{03}^2 + \sum_b \frac{1}{12\pi^2} \left[p_{F_b} E_{F_b}^3 - \frac{m_b^{*2}}{2} \left(5p_{F_b} E_{F_b} \right. \right. \\ & \left. \left. - 3m_b^{*2} \ln \left(\frac{p_{F_b} + E_{F_b}}{m_b^*} \right) \right) \right] + \frac{1}{12\pi^2} \sum_l \left[p_{F_l} E_{F_l}^3 - \frac{m_l^2}{2} \left(5p_{F_l} E_{F_l} - 3m_l^2 \ln \left(\frac{p_{F_l} + E_{F_l}}{m_l} \right) \right) \right] \\ & + n\Sigma^r \end{aligned} \quad (5)$$

respectively with p_{F_j} , E_{F_j} denoting the Fermi momentum and Fermi energy of the j -th fermion in the system. Here the rearrangement term Σ^r arises due to the density dependence of coupling parameters (to maintain thermodynamic consistency) and is given by [76]

$$\Sigma^r = \sum_b \left[\frac{\partial g_{\omega b}}{\partial n} \omega_0 n_b + \frac{\partial g_{\phi b}}{\partial n} \phi_0 n_b - \frac{\partial g_{\sigma b}}{\partial n} \sigma n_b^s - \frac{\partial g_{\sigma^* b}}{\partial n} \sigma^* n_b^s + \frac{\partial g_{\rho b}}{\partial n} \rho_{03} \tau_{N3} n_b \right]. \quad (6)$$

The parameters at nuclear saturation density (n_0), saturation energy (E_0), incompressibility (K_0), skewness (Q_0), effective nucleon mass (m_N^*/m_N), symmetry energy (E_{sym}) and its slope L_{sym} are given in table 1.

n_0 (fm^{-3})	E_0 (MeV)	K_0 (MeV)	Q_0 (MeV)	E_{sym} (MeV)	L_{sym} (MeV)	m_N^*/m_N
0.152	-16.14	250.9	478.9	32.3	51.3	0.57

Table 1: The nuclear parameters at n_0

3 Dark matter model

Because of the unclear picture of the DM mass and interactions, theoretically many models of the DM are there that can be incorporated into viable beyond standard model theories. This matter can be fermionic or bosonic, self-interacting via attractive or repulsive potential or even non-interacting [9]. Following previous works [57, 66], we construct the DM model in the relativistic mean-field approach, considering ‘dark’ hadrons that self-interact via ‘dark scalar’ and ‘dark vector’ bosons. We consider fermionic DM with cases of no self-interactions, either scalar or vector self-interactions, or both. DM is assumed to interact with HM only gravitationally. The Lagrangian of DM is given by [66]:

$$\begin{aligned}\mathcal{L}_{DM} = & \bar{\psi}_D [\gamma_\mu (i\partial^\mu - g_{vd}V^\mu) - (m_D - g_{sd}\phi_D)]\psi_D + \frac{1}{2}(\partial_\mu\phi_D\partial^\mu\phi_D - m_{sd}^2\phi_D^2) \\ & - \frac{1}{4}V_{\mu\nu,D}V_D^{\mu\nu} + \frac{1}{2}m_{vd}^2V_{\mu,D}V_D^\mu\end{aligned}\quad (7)$$

Here ψ_D , ϕ_D , and V_D^μ represent the fermionic DM, ‘dark scalar meson’, and ‘dark vector meson’ respectively. m_D is the bare mass of the fermionic DM. m_{sd} and m_{vd} are the corresponding masses of the scalar and vector ‘dark mesons’ respectively. g_{sd} and g_{vd} are the corresponding coupling strengths. From this Lagrangian, the pressure, energy density, and number density of DM can be given as [54, 55, 57, 66, 77]

$$\varepsilon_{DM} = \frac{1}{\pi^2} \left[k_{FD} E_{FD}^3 - \frac{m_D^{*2}}{8} \left\{ k_{FD} E_{FD} + m_D^{*2} \ln \left(\frac{k_{FD} + E_{FD}}{m_D^*} \right) \right\} \right] + \frac{n_{DM}^2 c_v^2}{2} + \frac{m_{sd}^2 \phi_{D0}^2}{2}, \quad (8)$$

$$p_{DM} = \frac{1}{12\pi^2} \left[k_{FD} E_{FD}^3 - \frac{m_D^{*2}}{2} \left\{ 5k_{FD} E_{FD} - 3m_D^{*2} \ln \left(\frac{k_{FD} + E_{FD}}{m_D^*} \right) \right\} \right] + \frac{n_{DM}^2 c_v^2}{2} - \frac{m_{sd}^2 \phi_{D0}^2}{2}, \quad (9)$$

$$n_{DM} = \frac{k_{FD}^3}{3\pi^2} \quad (10)$$

where k_{FD} is Fermi momentum of DM particle and $E_{FD} = \sqrt{k_{FD}^2 + m_D^{*2}}$ its Fermi energy. m_D^* is the effective DM fermion mass, given by

$$m_D^* = m_D - g_{sd}\phi_{D0} \quad (11)$$

and ϕ_{D0} is [77]

$$\phi_{D0} = \frac{g_{sd}}{m_{sd}^2} \langle \bar{\psi}_D \psi_D \rangle = \frac{c_s^2}{g_{sd}} \times \frac{m_D^*}{2\pi^2} \left[k_{FD} E_{FD} - m_D^{*2} \ln \left(\frac{k_{FD} + E_{FD}}{m_D^*} \right) \right] \quad (12)$$

where $c_v = g_{vd}/m_{vd}$ and $c_s = g_{sd}/m_{sd}$ are the scalar and vector free parameters.

3.1 DM parameters

In this work, we construct DM EOSs by varying several free parameters- the free DM particle mass, m_D , the scalar and vector free parameters, c_s , and c_v . Since these parameters can take on arbitrary values, we limit them as follows:

- m_D is taken in the range of 0.2 – 2.0 GeV in intervals of 0.1 GeV. This range of DM particle masses is arbitrary but gives pure DM stars with mass in the order of solar mass [56, 78].
- Ranges of c_s and c_v are arbitrary. Although [66] explores c_s and c_v in the ranges of 1 – 7 GeV⁻¹ and 10 – 14 GeV⁻¹ respectively, we vary both of them from 0 – 50 GeV⁻¹ in steps of 2 GeV⁻¹. With hyperons we choose the value of c_v up to 100 GeV⁻¹.

- Not all combinations of c_s , c_v and m_D give valid EOSs. We discard EOSs where the $dp/d\varepsilon$ becomes negative or where pressure itself becomes negative.
- As will be explained in section 4.3, to obtain the DM EOS, we need to fix another parameter- the total DM mass fraction, M_f . This is the ratio of the mass of DM in a star to the total mass of the star. We vary this parameter from 1% – 20% in steps of 1%

4 Stellar Structure and Tidal Deformability

4.1 TOV equations

In our model, DM interacts with HM of the star only via gravitational interaction. Hence, the stellar structure of DM admixed NSs will be governed by the two-fluid stellar structure equations. The two fluids in our case are the HM and the DM. The equilibrium configurations of non-rotating relativistic stars are obtained by solving the Tolmann-Oppenheimer-Volkoff (TOV) equations with the spherically symmetric line element

$$ds^2 = -e^{2\Phi} dt^2 + e^{2\Lambda} dr^2 + r^2 d\theta^2 + r^2 \sin^2 \theta d\phi^2 \quad (13)$$

The single fluid TOV equations are

$$\begin{aligned} \frac{dm}{dr} &= 4\pi r^2 \varepsilon \\ \frac{d\Phi}{dr} &= \frac{m + 4\pi r^3 p}{r(r - 2m)} \\ \frac{dp}{dr} &= -(p + \varepsilon) \frac{d\Phi}{dr} \\ \Lambda(r) &= -\frac{1}{2} \ln \left(1 - \frac{2m}{r} \right) \end{aligned} \quad (14)$$

where m is the mass enclosed by the radius r , Φ and Λ are the metric functions, p and ε are the pressure and energy density respectively.

In the two-fluid model the TOV equations become [66]

$$\begin{aligned} \frac{dm_1}{dr} &= 4\pi r^2 \varepsilon_1 \\ \frac{dm_2}{dr} &= 4\pi r^2 \varepsilon_2 \\ \frac{d\Phi}{dr} &= \frac{(m_1 + m_2) + 4\pi r^3 (p_1 + p_2)}{r(r - 2(m_1 + m_2))} \\ \frac{dp_1}{dr} &= -(p_1 + \varepsilon_1) \frac{d\Phi}{dr} \\ \frac{dp_2}{dr} &= -(p_2 + \varepsilon_2) \frac{d\Phi}{dr} \\ \Lambda(r) &= -\frac{1}{2} \ln \left\{ 1 - \frac{2(m_1 + m_2)}{r} \right\} \end{aligned} \quad (15)$$

These are now five coupled differential equations that need to be solved simultaneously, where the subscripts 1, 2 label the two fluids. At some point during the integration of these equations, the pressure of one of the fluids will vanish, marking the radius R_i of fluid i . The integration is then switched to solve the single fluid-structure equations (14). When the pressure of the remaining fluid vanishes, we get the final stellar structure. We get the total mass of the star as the sum of the masses of the two fluids. When the radius of the DM is less than that of the other fluid, the star has a DM core, while if the radius is greater, the star has a DM halo surrounding it.

4.2 Dimensionless tidal deformability

A compact star in a binary experiences deformation due to the external quadrupolar field of the companion. Tidal deformability parameter is the measure of the response in terms of the deformability of the star to the external quadrupolar field and defined as the ratio of the induced mass quadrupole moment Q to external perturbing tidal field \mathcal{E} as [56, 79]

$$\lambda = -\frac{Q}{\mathcal{E}} = \frac{2}{3}k_2R^5 \quad (16)$$

where

$$\begin{aligned} k_2 = & \frac{8}{5}C^5(1-2C^2)[2-y_R+2C(y_R-1)] \times \{2C(6-3y_R+3C(5y_R-8)) \\ & + 4C^3[13-11y_R+C(3y_R-2)+2C^2(1+y_R)] \\ & + 3(1-2C^2)[2-y_R+2C(y_R-1)]\ln(1-2C)\}^{-1}. \end{aligned} \quad (17)$$

$C = M/R$ is the compactness parameter with M and R being the mass and radius of the star respectively. Here y is the solution to the differential equation

$$y' = -\frac{1}{r}(y^2 + ye^{2\Lambda}(1 + 4\pi r^2(p - \varepsilon)) + Qr^2) \quad (18)$$

where

$$Q = 4\pi e^{2\Lambda} \left(5\varepsilon + 9p + (p + \varepsilon) \frac{d\varepsilon}{dp} \right) - \frac{6e^{2\Lambda}}{r^2} - 4\Phi'^2 \quad (19)$$

and y_R is the value of y at the surface of the star. From here, the dimensionless tidal deformability is defined as

$$\Lambda = \frac{\lambda}{M^5} = \frac{2}{3} \frac{k_2}{C^5} \quad (20)$$

And the binary tidal deformability $\tilde{\Lambda}$ is

$$\tilde{\Lambda} = \frac{16}{13} \frac{(12q+1)\Lambda_1 + (12+q)q^4\Lambda_2}{(1+q)^5}, \quad (21)$$

here, q is the mass ratio of the secondary component to the primary component. For two-fluid, DM admixed stars, the modifications in these equations are [66]:

$$\varepsilon \rightarrow \varepsilon_1 + \varepsilon_2 \quad p \rightarrow p_1 + p_2 \quad (p + \varepsilon) \frac{d\varepsilon}{dp} \rightarrow (p_1 + \varepsilon_1) \frac{d\varepsilon_1}{dp_1} + (p_2 + \varepsilon_2) \frac{d\varepsilon_2}{dp_2} \quad (22)$$

4.3 Dependence on DM parameters

With this two-fluid model, to get the mass-radius (M-R) relation of the star, first, we need to fix the DM fraction present in the star. We fix the DM fraction by mass as

$$M_f = \frac{M(DM)}{M(DM) + M(HM)} \quad (23)$$

Here $M(DM)$ represents the total mass of the DM in the star, and $M(HM)$ means the same for HM. We use DDME2 density-dependent parametrization for HM in this work [80]. The mass fraction of DM in a particular star is determined completely by the central energy densities of the HM and DM. Since this fraction cannot be known until the structure equations are solved, we employ a root-finding algorithm to find the DM's central energy density, which would give the required mass fraction for a given central energy density of HM. As the two matter components do not interact with each other, two different spheres are formed. Depending on the central density and EOS of DM, the NS can have a DM core surrounded by HM, or have a DM halo surrounding an HM star. In the case of the M-R relations, we take the radius of the star to be the observable radius of the star (radius of HM) because the electromagnetic probes used to find the radius of the star cannot detect the DM halo [81, 82]. However, when calculating the tidal deformability, we take the star's radius to be the maximum radius among the radius of HM and DM. This is because the DM halo would have a gravitational influence affecting the spacetime geometry [81].

For the EOS of the crust, we use the Baym-Pethick-Sutherland (BPS) model as given in reference [83]. To observe the effects of different parameters on M-R relations and tidal deformability, we choose a few values from the set of parameters as mentioned in section 3.1. For a fixed fraction $M_f = 10\%$ of DM with particle mass $m_D = 0.6$ GeV, the effect of scalar and vector interactions in the dark sector is shown in the left panels of figure 1. In the upper panels, we show pure nucleonic matter, and in the lower panels, hyperons are also included. For obvious reasons, in the presence of hyperons, the EOS of matter becomes soft, reducing the maximum attainable mass and tidal deformability, as evident from a comparison of upper and lower panels. Here, the square marker shows the transition from DM core to DM halo as mass decreases and vice versa for the transition with the circle marker. For example, for $c_s = c_v = 10$ GeV⁻¹, $m_D = 0.6$ GeV and $M_f = 10\%$, every star with a mass above the square marker and below the circle marker has a DM core. Keeping the same vector interaction (c_v), with increasing scalar interaction (c_s) DM EOS becomes softer. Similarly, keeping c_s the same, DM EOS becomes stiffer with an increase of c_v . Stars having stiffer DM EOS would have DM distributed widely, making them less compact. That is why the DM halo is formed for these stars within the mass range as shown. This less dense DM causes a larger radius of the NS as compared to the NSs having DM cores due to dense DM; this is evident from the left panel of figure 1. In the sub-right panels, we show the variation of Λ with mass for different values of c_s and c_v . Again, for stiffer DM EOS, the tidal deformability is large as compactness is small. The horizontal dotted line represents the minimum $2 M_\odot$ maximum mass bound from the M-R relation. For the fixed scalar and vector interactions, with $c_s = c_v = 30$ GeV⁻¹ the variation in M-R relation for different M_f are shown in the right panel of figure 1 by solid curves for $m_D = 0.4$ GeV and by dashed curves for $m_D = 0.8$ GeV. Here, we observe that for larger m_D , the DM EOS becomes softer, mostly forming DM cores, and for smaller m_D only DM halos are formed for the given combinations. For the softest DM EOS ($c_s = c_v = 30$ GeV⁻¹,

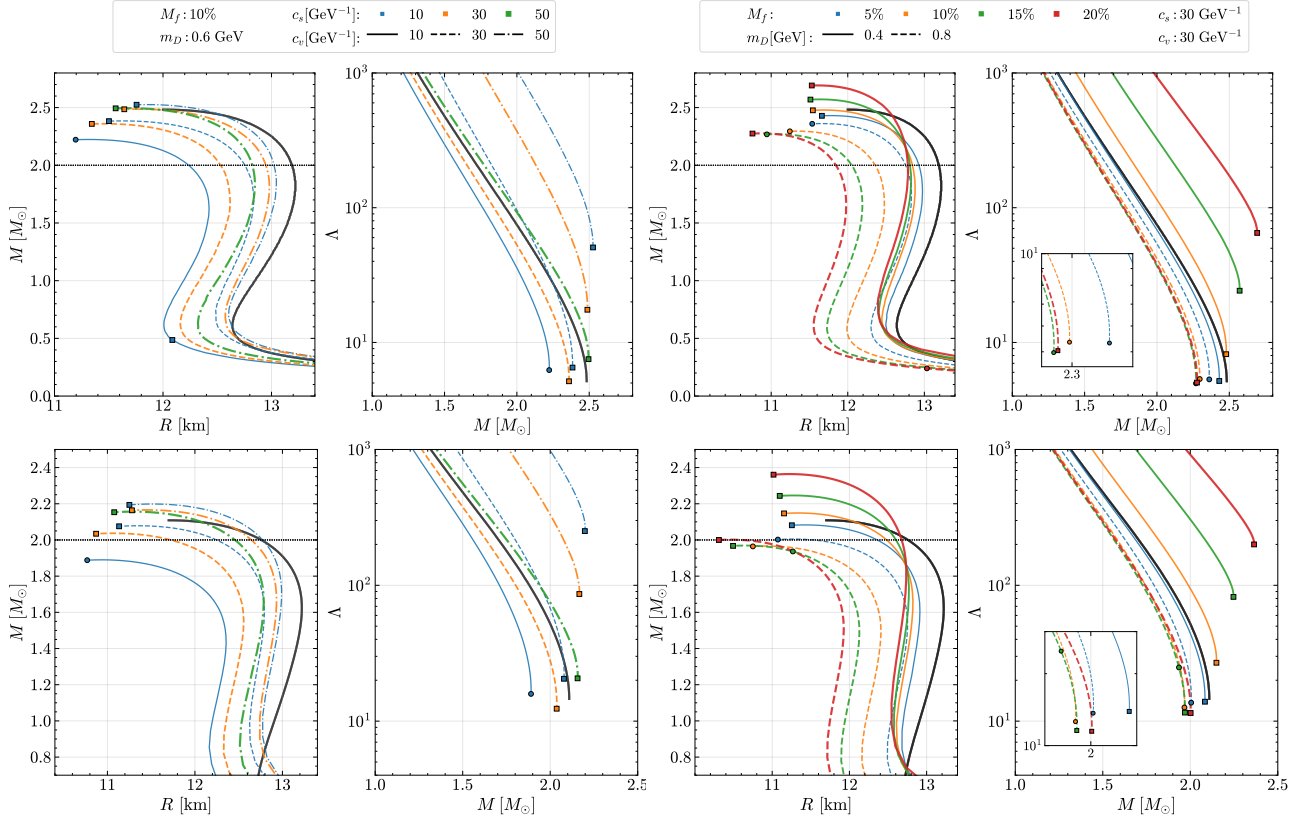


Figure 1: (colors are available in the online version) Effects of varying the DM parameters on the M-R and tidal deformability with stellar mass relations of DM admixed stars. The upper panels are for pure nuclear matter, and the lower panels also include hyperons. The thick, solid black line is for pure BM. While decreasing mass, the square marker shows the conversion of DM core to halo and vice versa for the circle marker. The horizontal line in the M-R graph is for $2M_\odot$.

$m_D = 0.6$ GeV and $M_f = 10\%$), we observe the transition from DM core to halo while stellar mass is increasing. In other cases with smaller M_f a DM core is formed. In cases of DM halo, to get a larger M_f , the quantity of DM needs to increase. This increases the maximum mass of the star. In cases of DM core, lesser quantities of HM are needed for greater M_f . As a result, the maximum mass of the star decreases. This behavior is also evident from the variation of Λ , which is shown in the sub-right panel of figure 1. We observe that for smaller m_D when DM halo is formed, increasing M_f decreases the compactness, increasing Λ ; while, for larger m_D and cases of DM cores, increasing M_f increases compactness, decreasing Λ . DM halos are more likely to be formed for lower m_D and higher M_f . These conclusions are similar to those obtained by ref. [78]. By fixing chirp mass and considering all the possible mass combinations such that the sum of both masses range is within the total mass range of GW170817 event, the tidal deformability of primary and secondary components is shown in figure 2. The shaded region represents the $\hat{\Lambda}$ less than 720 as given by the reference [84]. Curves with softer EOSs like lower c_v , higher c_s , and higher values of M_f and m_D lie within the limit. Results remain almost the same with the appearance of hyperons due to a very small fraction of hyperons at this energy density. The equilibrium speed of sound ($c_e = \sqrt{dp/d\varepsilon}$) is depicted in figure 3 with energy

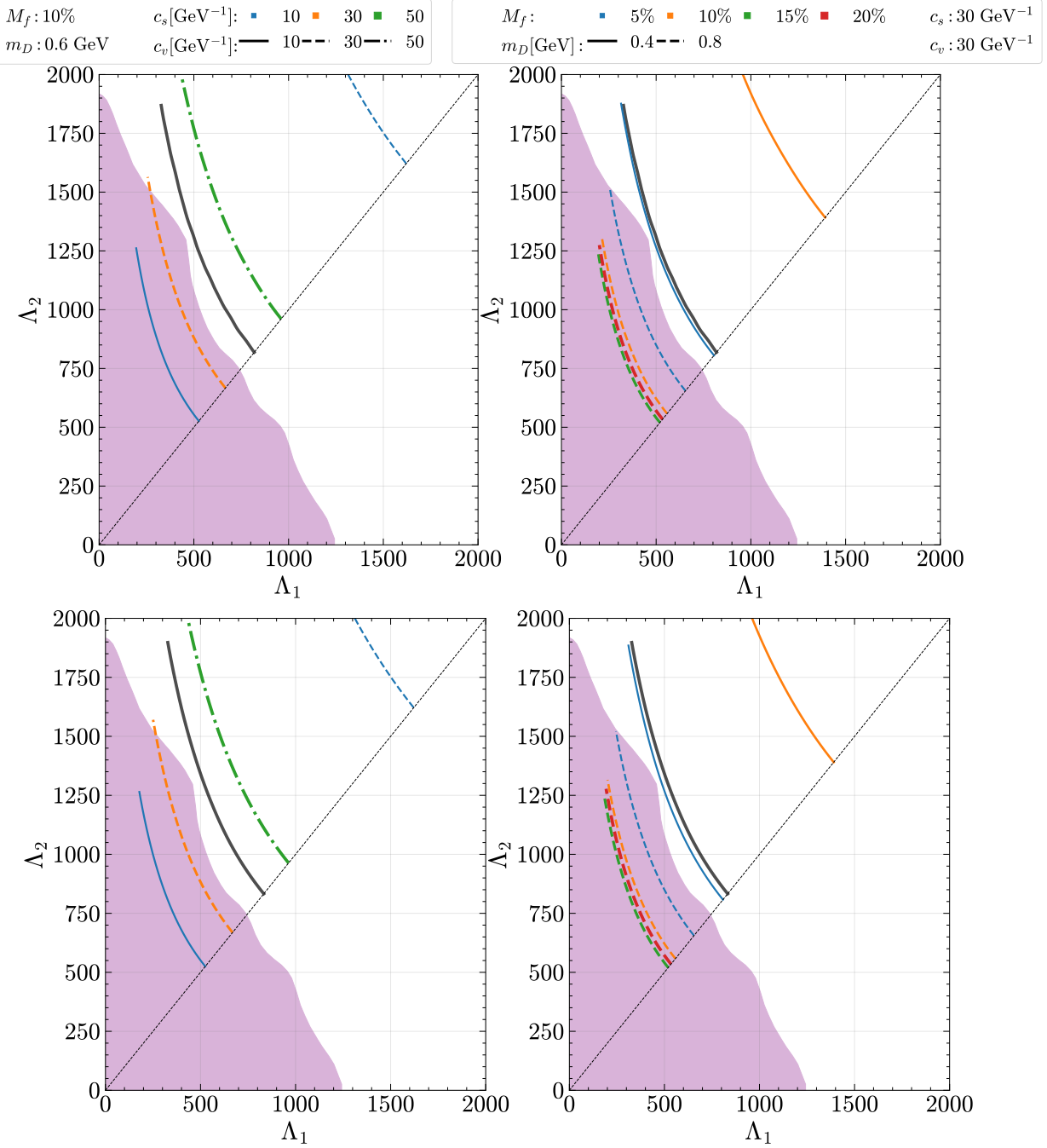


Figure 2: (colors are available in the online version) Effects of varying the DM parameters on the combinations of tidal deformability of primary and secondary mass in DM admixed stars. The upper panels are for pure nuclear matter, and the lower panels also include hyperons. The thick, solid black line is for pure BM.

density for the maximum mass configuration corresponding to each set of parametrization. c_e is within the range $0 \leq c_e \leq c$ obtained from causality and thermodynamic conditions [85]. As we noticed in previous results, with the same parameters, the maximum mass star with 10% DM fraction has a DM core, and with 20% DM fraction, a DM halo surrounds it. In the left panel, there are some sudden drops in the graph due to the appearance of another fluid; for

example, the dashed curve for 20% DM (orange) converts into a solid curve when HM gets mixed with DM, there is a drop due to softer EOS of HM with respect to DM EOS. In the right panel, an additional drop can be noticed at an energy density of approximately 400 MeV fm⁻³ due to the appearance of hyperons with nucleons. The appearance of hyperons makes EOS soft, or it reduces the slope $dp/d\varepsilon$ suddenly [86, 87]. The presence of DM significantly affects the speed of sound.

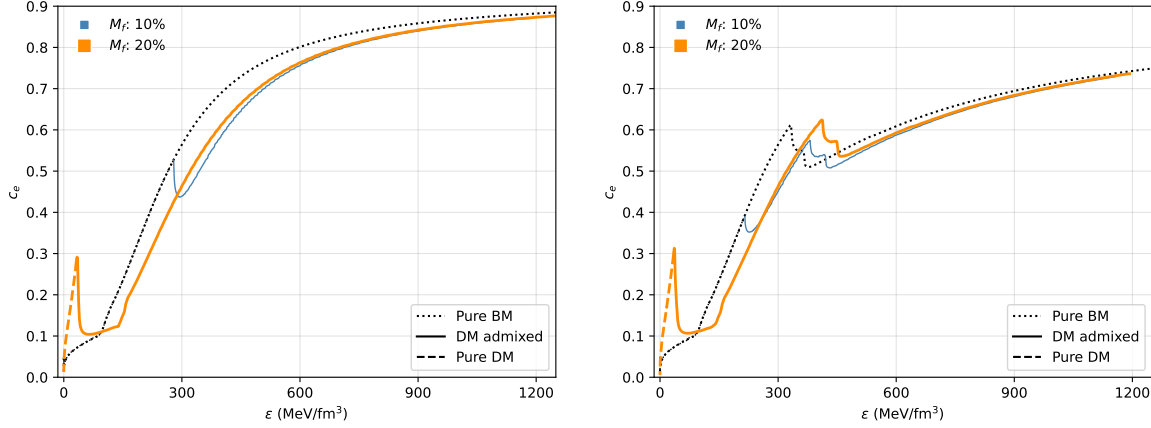


Figure 3: (colors are available in the online version) Equilibrium speed of sound plotted against average density and energy density in the star for maximum mass configuration. The left panel is for pure nuclear matter, and the right panel also includes hyperons. The value of both parameters c_s and c_v is 30 GeV⁻¹ and dark matter particle mass is 0.8 GeV.

5 Non Radial Modes

5.1 Equations governing non-radial modes

Due to external or internal perturbations in the star, non-radial oscillations are generated. Here we concentrate on the quadrupolar ($l = 2$) f- and p1-mode. These modes have pressure as the restoring force and radial node numbers 0 and 1, respectively. We calculate the mode frequencies with the relativistic Cowling approximation. Although the numerical values of frequencies in the Cowling approximation differ from those in the full GR calculations (by up to 30% for f-, and $\sim 15\%$ for p1- [88, 89]), the qualitative results are not affected much.

We follow the formalism given in [90, 91]. Since we're working within the relativistic Cowling approximation, the metric perturbations are neglected. The fluid perturbations are governed by the fluid Lagrangian displacement vector, which is taken to be

$$\xi^i = \left(\frac{e^{-\Lambda}}{r^2} W(t, r) Y_{lm}(\theta, \phi), \frac{-V(t, r)}{r^2} \partial_\theta Y_{lm}(\theta, \phi), \frac{-V(t, r)}{r^2 \sin^2 \theta} \partial_\phi Y_{lm}(\theta, \phi) \right) \quad (24)$$

Here W and V are variables of the fluid perturbation. Their relations are obtained by taking a variation of the energy-momentum conservation law $\delta(\nabla_\nu T^{\mu\nu})$ which reduces to $\nabla_\nu \delta T^{\mu\nu}$ in the Cowling approximation. Here $\delta T^{\mu\nu}$ is given by [91]

$$\delta T^{\mu\nu} = \begin{bmatrix} -\delta\varepsilon & (p+\varepsilon)U^0U^1 & (p+\varepsilon)U^0U^2 & (p+\varepsilon)U^0U^3 \\ (p+\varepsilon)U^1U^0 & \delta p & 0 & 0 \\ (p+\varepsilon)U^2U^0 & 0 & \delta p & 0 \\ (p+\varepsilon)U^3U^0 & 0 & 0 & \delta p \end{bmatrix} \quad (25)$$

U^μ is obtained by simply taking a temporal derivative of equation (24) and noting that the time-like component is the same as that of the unperturbed four velocity for a static perfect fluid in the metric given by equation (13): $U^0 = e^{-\Phi}$

$$U^\mu = \left(e^{-\Phi}, \frac{e^{-\Lambda}}{r^2} \partial_t W Y_{lm}, \frac{-\partial_t V}{r^2} \partial_\theta Y_{lm}, \frac{-\partial_t V}{r^2 \sin^2 \theta} \partial_\phi Y_{lm} \right) \quad (26)$$

The Eulerian variations of energy density and pressure are given by [91]

$$\delta\varepsilon = (p+\varepsilon) \frac{\Delta n}{n} - \varepsilon' \xi^r \quad \delta p = \gamma p \frac{\Delta n}{n} - p' \xi^r \quad (27)$$

where

$$\frac{\Delta n}{n} = - \left(e^{-\Lambda} \frac{W'}{r^2} + \frac{l(l+1)}{r^2} V \right) Y_{lm} \quad (28)$$

is the lagrangian variation in number density, and

$$\gamma = \frac{\partial \ln p}{\partial \ln n} = \frac{p+\varepsilon}{p} \frac{\partial p}{\partial \varepsilon} \quad (29)$$

is the adiabatic compressibility index. The dash represents the derivative with respect to r . W and V are assumed to have a harmonic time dependence, i.e., $W(t, r) = W(r)e^{i\omega t}$ and $V(t, r) = V(r)e^{i\omega t}$. We now start framing the perturbation equations following the procedure given in [90]. We substitute the perturbed variables and four-velocity in equation (25), and take the covariant divergence of the perturbed energy momentum tensor for two free indices $\mu = r, \theta$. Throughout the derivation, we use

$$p' = -\Phi'(p+\varepsilon) \quad \text{and} \quad \frac{p'}{p+\varepsilon} = -\Phi'$$

both of which are valid in the two-fluid case, with the singular terms replaced by the total ones, since from equation (15):

$$\begin{aligned} p'_1 + p'_2 &= -\Phi'(p_1 + \varepsilon_1 + p_2 + \varepsilon_2) = -\Phi'(p+\varepsilon) \quad \text{and,} \\ \frac{p'_1 + p'_2}{p_1 + \varepsilon_1 + p_2 + \varepsilon_2} &= \frac{-(p_1 + \varepsilon_1)\Phi' - (p_2 + \varepsilon_2)\Phi'}{p_1 + \varepsilon_1 + p_2 + \varepsilon_2} = -\Phi' \end{aligned} \quad (30)$$

To remove the dependence of γ , we use

$$\frac{p'}{\gamma p} = \frac{p'}{p+\varepsilon} \frac{\partial \varepsilon}{\partial p} = -\Phi' \frac{\partial \varepsilon}{\partial p}$$

which is easily obtained from equation (29). Making all these substitutions, we finally get:

$$W' = \frac{\partial \varepsilon}{\partial p} [\omega^2 r^2 e^{\Lambda-2\Phi} V + \Phi' W] - e^\Lambda l(l+1)V \quad (31)$$

$$V' = 2\Phi' V - \frac{e^\Lambda}{r^2} W + \left(\frac{d\varepsilon}{dp} - \frac{\partial \varepsilon}{\partial p} \right) \left[\Phi' V + \frac{e^{-\Lambda+2\Phi}}{\omega^2 r^2} \Phi'^2 W \right] \quad (32)$$

These are the oscillation mode equations. As a check of their correctness, note that if we take $\frac{d\varepsilon}{dp} = \frac{\partial \varepsilon}{\partial p}$, these equations reduce to those of [90]

$$\begin{aligned} W' &= \frac{d\varepsilon}{dp} [\omega^2 r^2 e^{\Lambda-2\Phi} V + \Phi' W] - e^\Lambda l(l+1)V \\ V' &= 2\Phi' V - \frac{e^\Lambda}{r^2} W \end{aligned} \quad (33)$$

Moreover, for stars with a temperature or composition gradient, these equations are the same as eqs. (25) and (26) of [92] with the transformations $\nu \rightarrow 2\Phi$, $\lambda \rightarrow 2\Lambda$ for the line element, and

$$\mathbb{W} \rightarrow -r^{-(l+1)} W \quad \text{and} \quad \mathbb{U} \rightarrow r^{-l} e^{-2\Phi} V$$

where \mathbb{W} and \mathbb{U} are the fluid perturbation variables in [92] and W and V are the corresponding variables in this work.

The boundary conditions at the center of the star are $W(r) = Ar^{l+1}$ and $V(r) = -Ar^l/l$, where A is an arbitrary constant. The surface boundary condition ($r = R$) is [90] $\Delta p = \gamma p \frac{\Delta n}{n} = 0$ which from equation (28) gives

$$\omega^2 R^2 e^{\Lambda(R)-2\Phi(R)} V(R) + \Phi'|_{r=R} W(R) = 0 \quad (34)$$

In the two-fluid case, the only modification is in the $\frac{d\varepsilon}{dp}$ term. Using equation (30), we get

$$\frac{d\varepsilon}{dp} = \frac{d(\varepsilon_1 + \varepsilon_2)}{d(p_1 + p_2)} = \frac{d\varepsilon_1}{dp_1} \frac{p'_1}{p'_1 + p'_2} + \frac{d\varepsilon_2}{dp_2} \frac{p'_2}{p'_1 + p'_2} \quad (35)$$

$$\frac{d\varepsilon}{dp} = \frac{p_1 + \varepsilon_1}{p_1 + \varepsilon_1 + p_2 + \varepsilon_2} \frac{d\varepsilon_1}{dp_1} + \frac{p_2 + \varepsilon_2}{p_1 + \varepsilon_1 + p_2 + \varepsilon_2} \frac{d\varepsilon_2}{dp_2} \quad (36)$$

Since we don't consider temperature or composition gradients, the adiabatic sound speed equal to the equilibrium sound speed. Thus, equation (33), along with the above boundary conditions, are the equations used in this work. Once the central energy densities for HM and DM for a particular mass fraction have been identified, we solve the oscillation mode equations to find the frequency ω subject to boundary conditions. We start with an initial guess for ω and integrate equation (33). We then check if that value of ω satisfies equation (34). If not, the guess of ω is improved via the Newton-Raphson algorithm. The lowest root of equation (33) which satisfies the boundary conditions, ω , is the frequency corresponding to the f -mode. The next highest root is the first (p_1 -mode) in a family of pressure modes with ever-increasing frequency and radial node numbers. We check the radial node number to classify the modes by counting the number of times W and V are trivial inside the star.

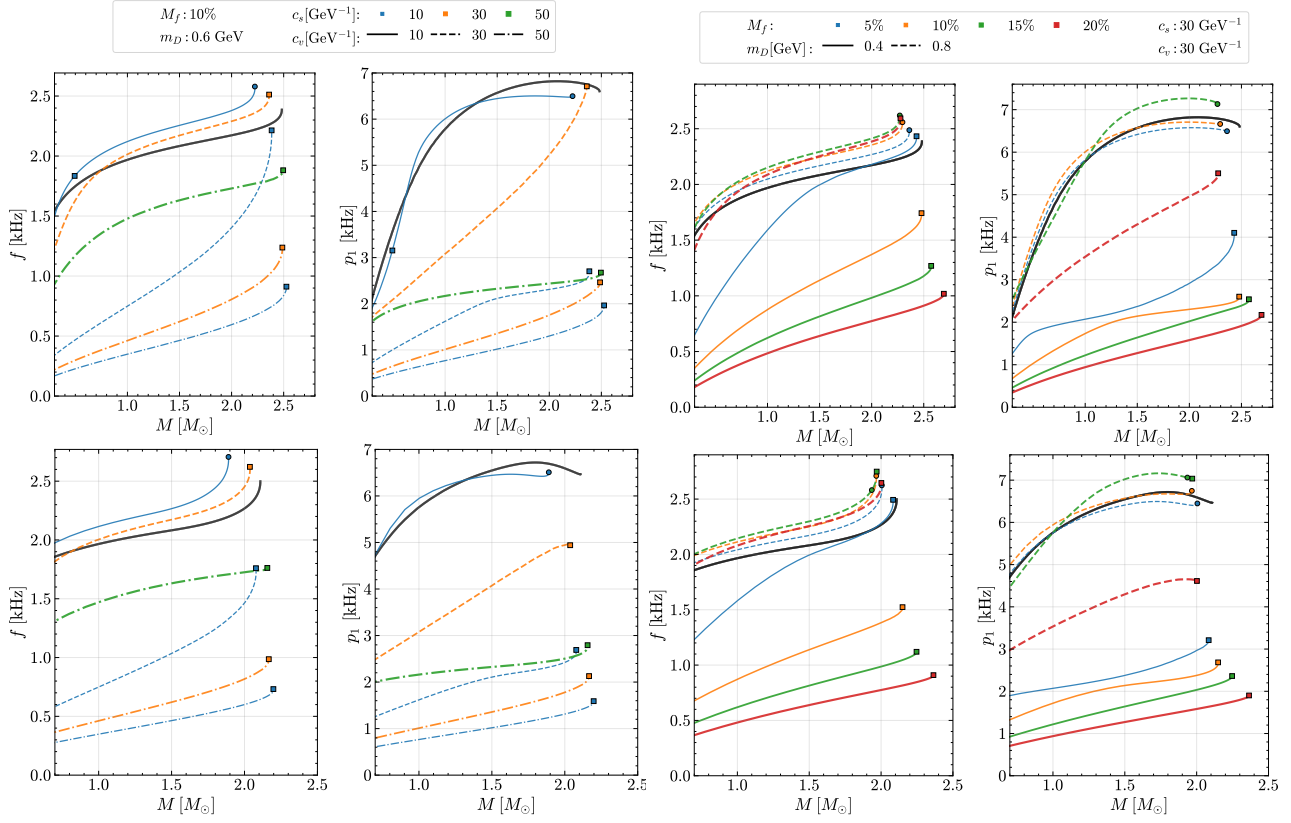


Figure 4: (colors are available in the online version) Effects of varying the DM parameters on the f and p_1 mode frequency with stellar mass in DM admixed stars. The upper panels are for pure nuclear matter, and the lower panels for matter with hyperons. The thick, solid black line is for pure BM. While decreasing mass, the square marker shows the conversion of DM core to halo and vice versa for the circle marker.

5.2 Dependence on DM parameters and the hyperons presence

For the same DM parameters as in section 4.3, we see the effects on the non-radial mode frequencies. Figure 4 shows the variation of f - and p_1 -modes frequencies with stellar mass for different parametrizations and M_f of DM. As we have seen larger values of c_s for a fixed c_v make the matter in the star softer, the f - and p_1 -mode frequency increases while larger values of c_v for a fixed c_s have the opposite effect. This is clear from the left panels of the figure 4. The effect on p_1 -mode frequencies is most notable since the frequencies can decrease a lot, even becoming comparable to the typical ranges of the f -mode frequency (1-3 kHz) by suitably varying the DM self-interaction strength. In the right panels of figure 4, we show the variation of non-radial mode frequencies with stellar mass for different m_D and M_f . For both the f - and p_1 -mode cases the variation of frequencies with DM mass fraction is sensitive to whether the star has a DM halo or core. The mode frequencies are less for the DM halo and more for the DM core. When the stars have a DM halo, increasing M_f for a fixed m_d decreases the mode frequencies as it increases the stiffness, while for stars with DM core, the opposite effect is observed. Again, the effect on the p_1 -mode is much stronger than the effects on the f -mode. This is because p_1 -modes, due to the presence of a radial node, are much more sensitive to the distribution of matter in the star [93]. Presence of hyperons shows effects on non-radial

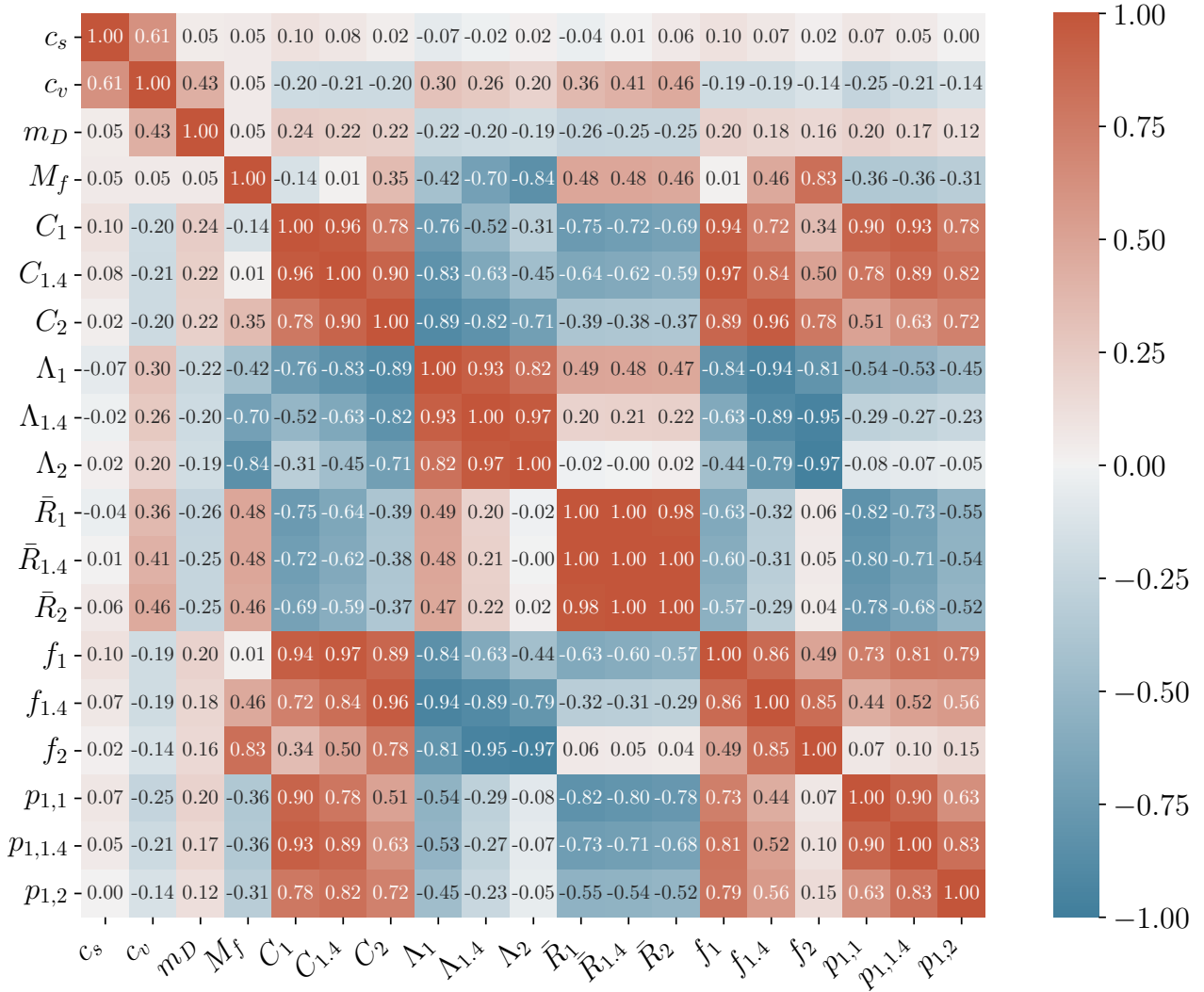


Figure 5: (colors are available in the online version) Correlation matrix showing the correlations amongst the DM EOS parameters, stellar structure parameters, and the non-radial modes. Correlations are obtained after applying the minimum $2M_{\odot}$ maximum mass and $\tilde{\Lambda} \leq 720$ constraints. Hyperons are not included in HM EOS.

oscillation mode's frequency near the maximum mass. In this region, if the DM core exists inside the star, then the frequency of both modes increases more rapidly than the DM halo.

5.3 Correlation studies

We show the mutual dependence of these parameters by the correlations between them in figure 5. Since the effects of DM are heavily dependent on the combinations of the parameters c_s , c_v , m_D , and M_f , correlations with any one of these parameters is expected to be weak. However as expected, the mode frequencies are strongly correlated with the corresponding compactness. We define compactness as the total mass of the star ($M_{HM} + M_{DM}$) divided by the outermost radius of the star (radius of DM, R_{DM} in case of DM halo, and radius of HM, R_{HM} in case of DM core). The p_1 -modes have a stronger negative correlation with another parameter $\bar{R} = R_{DM}/R_{HM}$ as

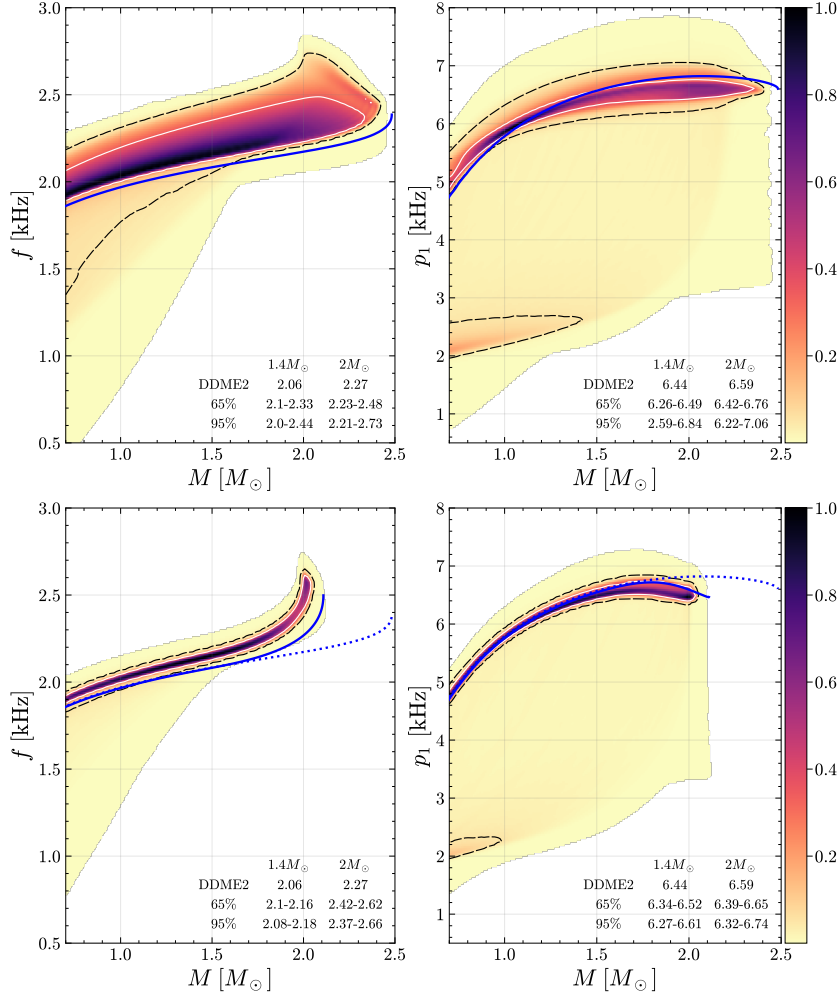


Figure 6: (colors are available in online version) PDFs for f - M and p_1 - M relations for valid stars. The upper panels are for pure nuclear matter, and the lower panels also include hyperons. The thick, solid blue line is for pure BM. In lower panels, the blue dotted line represents pure nuclear matter for comparison. The white solid and the black dashed lines represent the 65% and 95% regions, respectively. The f - M and p_1 - M relations for pure HM (DDME2) are shown with a solid blue line. Frequency values given by the confidence intervals at $1.4M_{\odot}$ and $2M_{\odot}$ are mentioned along with the frequency values for DDME2 at the same masses.

compared to f -modes. This parameter signifies the distribution of DM with respect to HM. This means that the p_1 -mode frequency is more sensitive to the presence of either a DM halo or a DM core than the f -mode. The behavior of the mode frequencies is very similar to that of the tidal deformability as shown in figure 1. When a particular variation of parameters increases the tidal deformability, a decrease in frequency is observed for the same variation. This suggests a negative correlation of the modes with tidal deformability and is indeed what we see in figure 5. Tidal deformability also shows a strong negative correlation with compactness.

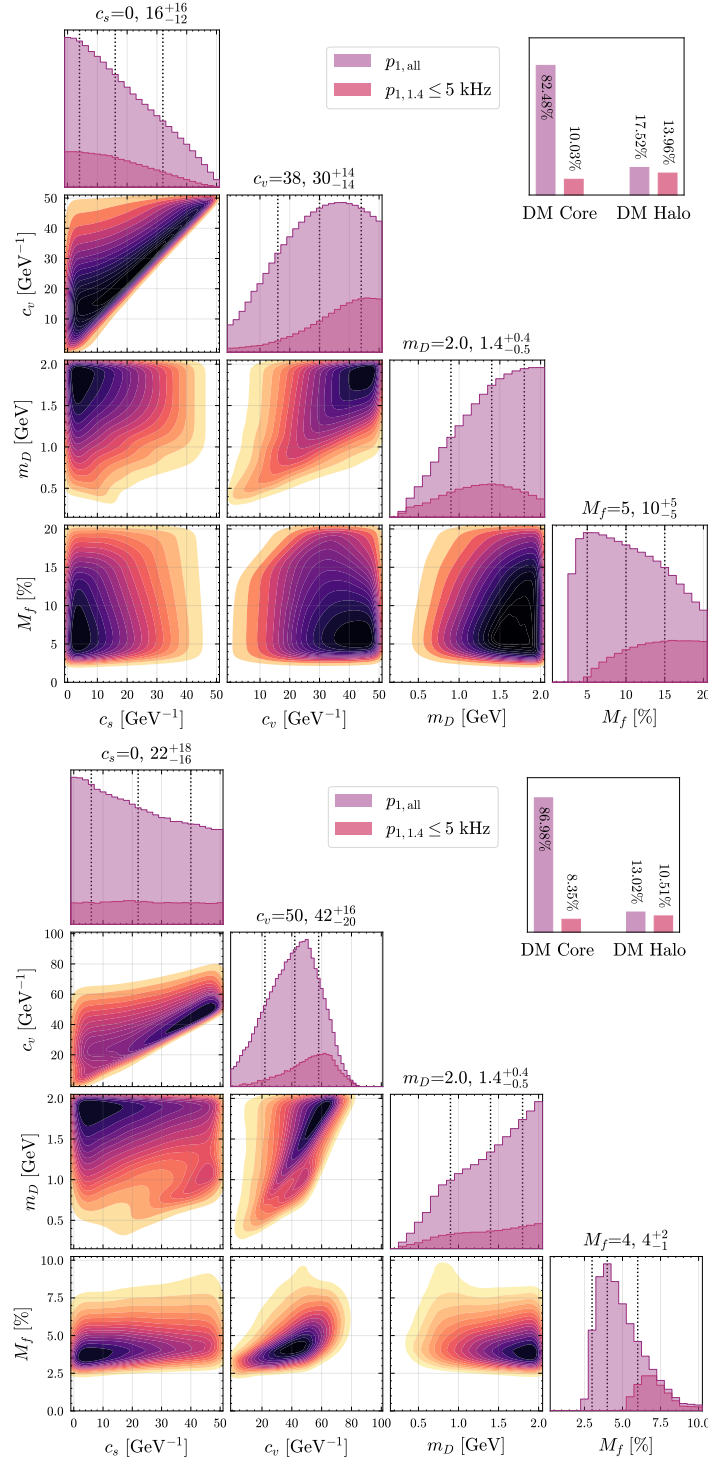


Figure 7: (colors are available in the online version) Corner plot with KDEs for the free parameters used in this work. The upper panel is for pure nuclear matter, and the lower panel is for nuclear matter with hyperons. The most probable values of each parameter, along with the median value with 1σ deviation, have been mentioned above the diagonal plots. The bar plot shows the percentage of stars with a DM core or halo. A darker color is used to mark the subset of low-frequency p_1 -modes

6 DM parameters from astrophysical observations

Next, we constrain the DM parameters for the DM admixed NS from the astrophysical observations of compact objects. We generate M-R relations and tidal deformability with all possible combinations of DM EOS parameters (c_s , c_v , m_D) and M_f , as mentioned in section 3.1 and then filter our EOSs by making them satisfy the mass constraint of at least $2M_\odot$ maximum mass and the tidal deformability constraint of $\tilde{\Lambda} \leq 720$. We call DM-admixed stars following these constraints ‘valid’. Once we have all combinations of parameters that follow these observational constraints, we show a KDE corner plot in figure 7. From the 2,56,880 total combinations, only 59,030 combinations give valid DM EOSs with $M - R$ and $\Lambda - M$ curves which follow the observational constraints we impose. We plot probability density plots for the f - and p_1 -modes in figure 6. For this, we first make a 250×250 grid and count the number of lines passing through each grid cell. Upon normalizing, we then have a density map of the f - M and p_1 - M plane. From this, the 65% (white solid line) and 95% (black dashed line) confidence intervals can be found. We have also shown the f - and p_1 - modes for DDME2 with no DM as a blue solid line. We find that the f -mode frequency for most DM admixed stars takes on a higher value than pure HM. For low mass stars, the f -mode frequency decreases a lot, with a minimum of around 1.5 kHz at $1.4 M_\odot$. However, the change in the p_1 -mode frequency is much more significant. Although the 65% confidence interval encloses the p_1 -mode for pure HM, there is a distinct low-frequency region for the 95% confidence interval. This frequency, between $1 - 3 \text{ kHz}$ is the typical frequency range of f -modes. The lowest p_1 -mode frequency at $1.4M_\odot$ is around 2.1 kHz. Further, due to the sensitivity of p_1 -modes to the DM distribution, the spread in their frequencies is much larger than that of the f -modes. In lower panels, the inclusion of heavier baryons reduces the maximum mass of neutron stars, and the presence of DM further exacerbates this reduction. We know that softer EOSs result in higher oscillation frequencies. However, we exclude the very soft EOSs that would result in a maximum mass lower than $2 M_\odot$, as this restriction influences the maximum frequency value. Consequently, we obtain very narrow 65% and 95% confidence intervals for the frequencies of both f - and p_1 -modes. For a massive star with a mass of $2 M_\odot$, the 65% credible interval for the f -mode frequency ranges from 2.42 to 2.62 kHz, which is narrower than the range obtained with the pure nuclear matter EOS. The 95% credible region for a $1.4 M_\odot$ star is more confined, with the f -mode frequency ranging from 2.08 to 2.18 kHz. Additionally, the range of the p_1 -mode frequency with a 95% confidence interval narrows significantly to 6.27-6.61 kHz, compared to the previous range of 2.62-6.87 kHz for a $1.4 M_\odot$ star. This indicates that even for low-mass stars, the p_1 -mode frequency is high.

We find that the most probable (1σ) values for or DM parameters are $c_s = 0$ (4–32) GeV^{-1} , $c_v = 38$ (16–44) GeV^{-1} , $m_D = 2.0$ (0.9–1.8) GeV and $M_f = 5$ (5–15)%. Due to presence of hyperons the parameters becomes $c_s = 0$ (6–40) GeV^{-1} , $c_v = 50$ (22–58) GeV^{-1} , $m_D = 2.0$ (0.9–1.8) GeV and $M_f = 4$ (3–6)%. With hyperons, EOS becomes soft. Thus, higher values of c_v are more favorable for making EOS stiffer. So, values of c_v are considered maximum up to 100 GeV . Since increasing m_d already reduces the maximum attainable mass and softens the EOS, large c_s values are less probable. However, large c_v values are more probable since they stiffen the EOS, increasing the maximum mass. Here, it should be noted that the most probable values of the DM parameters depend on the HM EOS chosen. Softer HM EOSs will allow for stiffer DM EOSs and larger c_s values, which follow the constraints we imposed. So the range of DM parameters given here is only relevant for DDME2 EOS. Further,

since increasing m_D softens the DM-admixed star while increasing c_v stiffens it, we can get valid DM-admixed stars for very large values of m_D and c_v . As an example, a combination of $c_s = 0 \text{ GeV}^{-1}$, $c_v = 50 \text{ GeV}^{-1}$, $m_D = 50 \text{ GeV}$ and $M_f = 7\%$ gives a valid star. The maximum accretion of DM predicted in neutron stars is typically less than this mass fraction, as further accumulation could lead to gravitational instability and collapse into a black hole [11, 94]. However, self-interacting DM with strong vector interactions considered in this study exhibits stiff EOS and is comparable to nuclear matter. This stiffness can counteract the gravitational collapse, thereby preventing the formation of a black hole. Consequently, NS may sustain significantly higher DM fractions, potentially allowing for the presence of a surrounding DM halo. In this work, we have restricted ourselves to small m_D values.

The darker regions in the histogram correspond to the low frequency p_1 -modes. We find that most of our DM-admixed stars have DM cores. However, for stars with DM halo, most of them also have low-frequency p_1 -modes. This means that combinations that are more likely to form a DM halo, i.e. higher c_v , lower m_d , and large M_f are more likely to give low-frequency p_1 -modes.

7 Summary

We have studied the stellar structure and properties of non-radial oscillation frequencies of DM admixed NSs. We have considered the density-dependent RMF model for the normal HM of the NS and self-interacting but non-annihilating DM which interacts with HM only gravitationally. The DM admixed NS can naturally have a large range of masses and tidal deformabilities since the DM EOS is not constrained. On the other hand, the observed radius of compact objects is related to the extent of HM in the DM admixed NSs. Hence observed M-R relations of the compact objects can be used to constrain the theoretical models of DM admixed NS. Due to their extreme densities, NSs are likely to be excellent captors of particle DM [42]. However, if we assume that the astrophysical compact objects contain some fraction of DM, we can estimate some DM properties from astrophysical observations. For example, in our present study, from the observed lower bound of maximum attainable mass of the compact objects and the upper bound of tidal deformability from the binary star merger observations, we predict the maximum probable value of the DM self-interaction parameters and the DM particle mass within a specific model of NS. We also estimate the DM fraction within a DM admixed NS. We find that 5% is the most repeating value of the DM fraction parameter. The higher chemical potential of nucleons allows the presence of heavy baryons. For the comparison, we include hyperons and find the most probable value of DM fraction as 4%. Such a high dark matter fraction exceeds the maximum limit predicted by Bondi accretion models. However, it may be achievable for Fermion-Proca stars [95, 96], which we will try to explore in our future studies.

The existence of DM admixed NS compels us to study the NS properties which are also important for future GW observations. In light of this, we study the non-radial oscillation frequencies of DM admixed NSs. M-R and tidal deformability constraints help us to filter relevant DM parameters, and we predict the non-radial oscillation frequencies of DM admixed NS with these filtered parameters. We find that the f - and p_1 -mode frequencies are strongly correlated with compactness and distribution of DM. The f -mode frequency increases due to the presence of DM as compared to pure HM stars. But a different trend is observed with the p_1 -mode frequency (typically 4-7 kHz), as the range is more widespread, with frequencies

reducing up to the typical range of f -mode frequencies (1-3 kHz). After including hyperons, the 95% confidence interval range of p_1 - mode shrinks noticeably, and it becomes to 6-7 kHz for a 1.4 solar mass star. A majority of these low frequency p_1 -modes arise in stars with a DM halo and are more probable in low mass stars. Further, the p_1 -modes for low-mass stars are more sensitive to DM distribution (whether there is a DM core or DM halo) as compared to f -modes which is evident from our corner plots and correlation studies. An important conclusion of our paper is thus that the effect of DM capture by compact stars can be seen much more clearly from non-radial modes, especially the p_1 -modes.

Data Availability

The data used in the manuscript can be obtained at reasonable request from the corresponding author.

Acknowledgments

The authors acknowledge the financial support from the Science and Engineering Research Board (SERB), Department of Science and Technology, Government of India through Project No. CRG/2022/000069. The authors thank Ritam Mallick for some valuable suggestions and Kamal Krishna Nath for his input. The authors also want to thank the anonymous referee for enhancing the manuscript's quality through constructive comments.

References

- [1] Gianfranco Bertone, Dan Hooper, and Joseph Silk. Particle dark matter: evidence, candidates and constraints. *Phys. Rep.*, 405(5-6):279–390, January 2005.
- [2] J Aalbers, F Agostini, M Alfonsi, FD Amaro, C Amsler, E Aprile, L Arazi, Francesco Arneodo, P Barrow, L Baudis, et al. Darwin: towards the ultimate dark matter detector. *Journal of Cosmology and Astroparticle Physics*, 2016(11):017, 2016.
- [3] Rouven Essig, Aaron Manalaysay, Jeremy Mardon, Peter Sorensen, and Tomer Volansky. First direct detection limits on sub-gev dark matter from xenon10. *Phys. Rev. Lett.*, 109:021301, Jul 2012.
- [4] Sergey Alekhin, Wolfgang Altmannshofer, Takehiko Asaka, Brian Batell, Fedor Bezrukov, Kyrylo Bondarenko, Alexey Boyarsky, Ki-Young Choi, Cristóbal Corral, Nathaniel Craig, et al. A facility to search for hidden particles at the cern sps: the ship physics case. *Reports on Progress in Physics*, 79(12):124201, 2016.
- [5] CDMS II Collaboration, Z. Ahmed, D. S. Akerib, S. Arrenberg, C. N. Bailey, et al. Dark Matter Search Results from the CDMS II Experiment. *Science*, 327(5973):1619, March 2010.
- [6] E. Aprile et al. First Dark Matter Search Results from the XENON1T Experiment. *Phys. Rev. Lett.*, 119(18):181301, November 2017.

- [7] E. Aprile et al. First dark matter search with nuclear recoils from the xenonnT experiment. *Phys. Rev. Lett.*, 131:041003, Jul 2023.
- [8] M. Khlopov. What comes after the Standard Model? *Progress in Particle and Nuclear Physics*, 116:103824, January 2021.
- [9] Andrea Maselli, Pantelis Pnigouras, Niklas Grönlund Nielsen, Chris Kouvaris, and Kostas D. Kokkotas. Dark stars: Gravitational and electromagnetic observables. *Phys. Rev. D*, 96(2):023005, July 2017.
- [10] Chris Kouvaris and Niklas Grönlund Nielsen. Asymmetric dark matter stars. *Phys. Rev. D*, 92(6):063526, September 2015.
- [11] Arnaud de Lavallaz and Malcolm Fairbairn. Neutron stars as dark matter probes. *Phys. Rev. D*, 81(12):123521, June 2010.
- [12] Nicole F. Bell, Giorgio Busoni, Sandra Robles, and Michael Virgato. Thermalization and annihilation of dark matter in neutron stars. *J. Cosmol. Astropart. Phys.*, 2024(4):006, April 2024.
- [13] Chian-Shu Chen and Yen-Hsun Lin. Reheating neutron stars with the annihilation of self-interacting dark matter. *Journal of High Energy Physics*, 2018(8):69, August 2018.
- [14] Raghuveer Garani, Aritra Gupta, and Nirmal Raj. Observing the thermalization of dark matter in neutron stars. *Phys. Rev. D*, 103(4):043019, February 2021.
- [15] Yasunari Kurita and Hiroyuki Nakano. Gravitational waves from dark matter collapse in a star. *Phys. Rev. D*, 93:023508, Jan 2016.
- [16] Chris Kouvaris and Peter Tinyakov. Can neutron stars constrain dark matter? *Phys. Rev. D*, 82(6):063531, September 2010.
- [17] S Nussinov. Technocosmology—could a technibaryon excess provide a “natural” missing mass candidate? *Physics Letters B*, 165(1-3):55–58, 1985.
- [18] S.M. Barr, R. Sekhar Chivukula, and Edward Farhi. Electroweak fermion number violation and the production of stable particles in the early universe. *Physics Letters B*, 241(3):387–391, 1990.
- [19] Sven Bjarke Gudnason, Chris Kouvaris, and Francesco Sannino. Dark matter from new technicolor theories. *Phys. Rev. D*, 74(9):095008, November 2006.
- [20] Roshan Foadi, Mads T. Frandsen, and Francesco Sannino. Technicolor dark matter. *Phys. Rev. D*, 80(3):037702, August 2009.
- [21] Thomas A. Rytov and Francesco Sannino. Conformal windows of $SU(N)$ gauge theories, higher dimensional representations, and the size of the unparticle world. *Phys. Rev. D*, 76(10):105004, November 2007.
- [22] Francesco Sannino. Conformal Dynamics for TeV Physics and Cosmology. *arXiv e-prints*, page arXiv:0911.0931, November 2009.

- [23] Thomas A. Rytov and Francesco Sannino. Ultraminimal technicolor and its dark matter technicolor interacting massive particles. *Phys. Rev. D*, 78:115010, Dec 2008.
- [24] Francesco Sannino and Roman Zwicky. Unparticle and higgs boson as composites. *Phys. Rev. D*, 79:015016, Jan 2009.
- [25] Mads T. Frandsen and Francesco Sannino. Isotriplet technicolor interacting massive particle as dark matter. *Phys. Rev. D*, 81:097704, May 2010.
- [26] John March-Russell and Matthew McCullough. Asymmetric dark matter via spontaneous co-genesis. *J. Cosmol. Astropart. Phys.*, 2012(3):019, March 2012.
- [27] Mads T. Frandsen, Felix Kahlhoefer, Subir Sarkar, and Kai Schmidt-Hoberg. Direct detection of dark matter in models with a light Z' . *Journal of High Energy Physics*, 2011:128, September 2011.
- [28] Xin Gao, Zhaofeng Kang, and Tianjun Li. Origins of the isospin violation of dark matter interactions. *J. Cosmol. Astropart. Phys.*, 2013(1):021, January 2013.
- [29] Chiara Arina and Narendra Sahu. Asymmetric inelastic inert doublet dark matter from triplet scalar leptogenesis. *Nuclear Physics B*, 854(3):666–699, January 2012.
- [30] Matthew R. Buckley and Stefano Profumo. Regenerating a symmetry in asymmetric dark matter. *Phys. Rev. Lett.*, 108:011301, Jan 2012.
- [31] Randy Lewis, Claudio Pica, and Francesco Sannino. Light asymmetric dark matter on the lattice: $Su(2)$ technicolor with two fundamental flavors. *Phys. Rev. D*, 85:014504, Jan 2012.
- [32] Hooman Davoudiasl, David E. Morrissey, Kris Sigurdson, and Sean Tulin. Baryon destruction by asymmetric dark matter. *Phys. Rev. D*, 84:096008, Nov 2011.
- [33] Michael L. Graesser, Ian M. Shoemaker, and Luca Vecchi. Asymmetric WIMP dark matter. *Journal of High Energy Physics*, 2011:110, October 2011.
- [34] Nicole F. Bell, Kalliopi Petraki, Ian M. Shoemaker, and Raymond R. Volkas. Dark and visible matter in a baryon-symmetric universe via the affleck-dine mechanism. *Phys. Rev. D*, 84:123505, Dec 2011.
- [35] Clifford Cheung and Kathryn M. Zurek. Affleck-dine co-genesis. *Phys. Rev. D*, 84:035007, Aug 2011.
- [36] Jordi Casanellas and Ilídio Lopes. The Formation and Evolution of Young Low-mass Stars within Halos with High Concentration of Dark Matter Particles. *Astro. Phys. J.*, 705(1):135–143, November 2009.
- [37] Pat Scott, Malcolm Fairbairn, and Joakim Edsjö. Dark stars at the Galactic Centre - the main sequence. *Mon. Not. Roy. Astron. Soc.*, 394(1):82–104, March 2009.
- [38] Chris Kouvaris. WIMP annihilation and cooling of neutron stars. *Phys. Rev. D*, 77(2):023006, January 2008.

- [39] Matthew McCullough and Malcolm Fairbairn. Capture of inelastic dark matter in white dwarves. *Phys. Rev. D*, 81(8):083520, April 2010.
- [40] Richard Brito, Vitor Cardoso, and Hirotada Okawa. Accretion of Dark Matter by Stars. *Phys. Rev. Lett.*, 115(11):111301, September 2015.
- [41] Tolga Güver, Arif Emre Erkoca, Mary Hall Reno, and Ina Sarcevic. On the capture of dark matter by neutron stars. *J. Cosmol. Astropart. Phys.*, 2014(5):013, May 2014.
- [42] Joseph Bramante and Nirmal Raj. Dark matter in compact stars, July 2023.
- [43] Ho-Sang Chan, Ming-chung Chu, Shing-Chi Leung, and Lap-Ming Lin. Delayed Detonation Thernuclear Supernovae with an Extended Dark Matter Component. *Astro. Phys. J.* , 914(2):138, June 2021.
- [44] S. C. Leung, M. C. Chu, and L. M. Lin. Dark Matter Admixed Type Ia Supernovae. *Astro. Phys. J.* , 812(2):110, October 2015.
- [45] Paolo Ciarcelluti and Fredrik Sandin. Have neutron stars a dark matter core? *Physics Letters B*, 695(1-4):19–21, January 2011.
- [46] S.-C. Leung, M.-C. Chu, and L.-M. Lin. Dark-matter admixed neutron stars. *Phys. Rev. D*, 84:107301, Nov 2011.
- [47] Z. Rezaei. Study of Dark-matter Admixed Neutron Stars Using the Equation of State from the Rotational Curves of Galaxies. *Astro. Phys. J.* , 835(1):33, January 2017.
- [48] John Ellis, Gert Hütsi, Kristjan Kannike, Luca Marzola, Martti Raidal, and Ville Vaskonen. Dark matter effects on neutron star properties. *Phys. Rev. D*, 97:123007, Jun 2018.
- [49] Moira I. Gresham and Kathryn M. Zurek. Asymmetric dark stars and neutron star stability. *Phys. Rev. D*, 99:083008, Apr 2019.
- [50] Maksym Deliyergiyev, Antonino Del Popolo, Laura Tolos, Morgan Le Delliou, Xiguo Lee, and Fiorella Burgio. Dark compact objects: An extensive overview. *Phys. Rev. D*, 99:063015, Mar 2019.
- [51] Ann E. Nelson, Sanjay Reddy, and Dake Zhou. Dark halos around neutron stars and gravitational waves. *Journal of Cosmology and Astroparticle Physics*, 2019(07):012, jul 2019.
- [52] H C Das, Ankit Kumar, Bharat Kumar, S K Biswal, Takashi Nakatsukasa, Ang Li, and S K Patra. Effects of dark matter on the nuclear and neutron star matter. *Monthly Notices of the Royal Astronomical Society*, 495(4):4893–4903, 05 2020.
- [53] Kilar Zhang, Guo-Zhang Huang, Jie-Shiun Tsao, and Feng-Li Lin. GW170817 and GW190425 as hybrid stars of dark and nuclear matter. *European Physical Journal C*, 82(4):366, April 2022.
- [54] Ben Kain. Dark matter admixed neutron stars. *Phys. Rev. D*, 103(4):043009, February 2021.

- [55] Payel Mukhopadhyay and Jürgen Schaffner-Bielich. Quark stars admixed with dark matter. *Physical Review D*, 93(8):083009, April 2016.
- [56] Kwing-Lam Leung, Ming-chung Chu, and Lap-Ming Lin. Tidal deformability of dark matter admixed neutron stars. *Physical Review D*, 105(12):123010, June 2022.
- [57] Swarnim Shirke, Suprovo Ghosh, Debarati Chatterjee, Laura Sagunski, and Jürgen Schaffner-Bielich. R-modes as a New Probe of Dark Matter in Neutron Stars, May 2023.
- [58] Swarnim Shirke, Bikram Keshari Pradhan, Debarati Chatterjee, Laura Sagunski, and Jürgen Schaffner-Bielich. Effects of Dark Matter on f -mode oscillations of Neutron Stars. *arXiv e-prints*, page arXiv:2403.18740, March 2024.
- [59] P. B. Demorest, T. Pennucci, S. M. Ransom, M. S. E. Roberts, and J. W. T. Hessels. A two-solar-mass neutron star measured using Shapiro delay. *Nature*, 467(7319):1081–1083, October 2010.
- [60] Ignazio Bombaci. The Hyperon Puzzle in Neutron Stars. In *Proceedings of the 12th International Conference on Hypernuclear and Strange Particle Physics (HYP2015)*, page 101002, January 2017.
- [61] S. Typel, G. Röpke, T. Klähn, D. Blaschke, and H. H. Wolter. Composition and thermodynamics of nuclear matter with light clusters. *Phys. Rev. C*, 81(1):015803, January 2010.
- [62] X. Roca-Maza, X. Viñas, M. Centelles, P. Ring, and P. Schuck. Relativistic mean-field interaction with density-dependent meson-nucleon vertices based on microscopical calculations. *Phys. Rev. C*, 84(5):054309, November 2011.
- [63] A. Taninah, S. E. Agbemava, A. V. Afanasjev, and P. Ring. Parametric correlations in energy density functionals. *Physics Letters B*, 800:135065, January 2020.
- [64] Vivek Baruah Thapa, Anil Kumar, and Monika Sinha. Baryonic dense matter in view of gravitational-wave observations. *Mon. Not. Roy. Astron. Soc.*, 507(2):2991–3004, October 2021.
- [65] Qian-Fei Xiang, Wei-Zhou Jiang, Dong-Rui Zhang, and Rong-Yao Yang. Effects of fermionic dark matter on properties of neutron stars. *Phys. Rev. C*, 89(2):025803, February 2014.
- [66] Arpan Das, Tuhin Malik, and Alekha C. Nayak. Dark matter admixed neutron star properties in light of gravitational wave observations: A two fluid approach. *Phys. Rev. D*, 105:123034, Jun 2022.
- [67] Fredrik Sandin and Paolo Ciarcelluti. Effects of mirror dark matter on neutron stars. *Astroparticle Physics*, 32(5):278–284, December 2009.
- [68] Kostas D. Kokkotas and Bernd G. Schmidt. Quasi-Normal Modes of Stars and Black Holes. *Living Reviews in Relativity*, 2(1):2, September 1999.

- [69] Lee Lindblom and Steven L Detweiler. The quadrupole oscillations of neutron stars. *Astrophysical Journal Supplement Series (ISSN 0067-0049)*, vol. 53, Sept. 1983, p. 73-92., 53:73–92, 1983.
- [70] Steven Detweiler and Lee Lindblom. On the nonradial pulsations of general relativistic stellar models. *The Astrophysical Journal*, 292:12–15, 1985.
- [71] K. D. Kokkotas, T. A. Apostolatos, and N. Andersson. The inverse problem for pulsating neutron stars: a ‘fingerprint analysis’ for the supranuclear equation of state. *Mon. Not. Roy. Astron. Soc.*, 320(3):307–315, January 2001.
- [72] Nikolaos Stergioulas, Andreas Bauswein, Kimon Zagkouris, and Hans-Thomas Janka. Gravitational waves and non-axisymmetric oscillation modes in mergers of compact object binaries. *Mon. Not. Roy. Astron. Soc.*, 418(1):427–436, November 2011.
- [73] Stamatis Vretinaris, Nikolaos Stergioulas, and Andreas Bauswein. Empirical relations for gravitational-wave asteroseismology of binary neutron star mergers. *Phys. Rev. D*, 101(8):084039, April 2020.
- [74] Cecilia Chirenti, Roman Gold, and M. Coleman Miller. Gravitational Waves from F-modes Excited by the Inspiral of Highly Eccentric Neutron Star Binaries. *Astro. Phys. J.*, 837(1):67, March 2017.
- [75] Norman K. Glendenning. *Compact Stars*. 1996.
- [76] Frank Hofmann, C. M. Keil, and H. Lenske. Application of the density dependent hadron field theory to neutron star matter. *Phys. Rev. C*, 64(2):025804, August 2001.
- [77] Grigoris Panotopoulos and Ilidio Lopes. The dark matter effect on realistic equation of state in neutron stars. *Physical Review D*, 96(8):083004, October 2017.
- [78] Hong-Ming Liu, Jin-Biao Wei, Zeng-Hua Li, G. F. Burgio, H. C. Das, and H. J. Schulze. Dark matter effects on the properties of neutron stars: compactness and tidal deformability. *arXiv e-prints*, page arXiv:2403.17024, March 2024.
- [79] Tanja Hinderer. Tidal love numbers of neutron stars. *The Astrophysical Journal*, 677(2):1216, apr 2008.
- [80] G. A. Lalazissis, T. Nikšić, D. Vretenar, and P. Ring. New relativistic mean-field interaction with density-dependent meson-nucleon couplings. *Phys. Rev. C*, 71(2):024312, February 2005.
- [81] Davood Rafiei Karkevandi, Soroush Shakeri, Violetta Sagun, and Oleksii Ivanytskyi. Tidal deformability as a probe of dark matter in neutron stars. In *The Sixteenth Marcel Grossmann Meeting on Recent Developments in Theoretical and Experimental General Relativity, Astrophysics and Relativistic Field Theories: Proceedings of the MG16 Meeting on General Relativity Online; 5–10 July 2021*, pages 3713–3731. World Scientific, 2023.
- [82] Soroush Shakeri and Davood Rafiei Karkevandi. Bosonic dark matter in light of the NICER precise mass-radius measurements. *Phys. Rev. D*, 109(4):043029, February 2024.

- [83] Gordon Baym, Christopher Pethick, and Peter Sutherland. The Ground State of Matter at High Densities: Equation of State and Stellar Models. *Astro. Phys. J.* , 170:299, December 1971.
- [84] B. P. Abbott, R. Abbott, T. D. Abbott, et al. Properties of the binary neutron star merger gw170817. *Phys. Rev. X*, 9:011001, Jan 2019.
- [85] Clifford E. Rhoades and Remo Ruffini. Maximum mass of a neutron star. *Phys. Rev. Lett.*, 32:324–327, Feb 1974.
- [86] Jürgen Schaffner-Bielich, Matthias Hanauske, Horst Stöcker, and Walter Greiner. Phase Transition to Hyperon Matter in Neutron Stars. *Phys. Rev. Lett.*, 89(17):171101, January 2002.
- [87] S. Weissenborn, D. Chatterjee, and J. Schaffner-Bielich. Hyperons and massive neutron stars: The role of hyperon potentials. *Nucl. Phys. A*, 881:62–77, May 2012.
- [88] Athul Kunjipurayil, Tianqi Zhao, Bharat Kumar, Bijay K. Agrawal, and Madappa Prakash. Impact of the equation of state on f - and p - mode oscillations of neutron stars. *Phys. Rev. D*, 106:063005, Sep 2022.
- [89] Tianqi Zhao and James M. Lattimer. Universal relations for neutron star f -mode and g -mode oscillations. *Phys. Rev. D*, 106:123002, Dec 2022.
- [90] Hajime Sotani, Nobutoshi Yasutake, Toshiki Maruyama, and Toshitaka Tatsumi. Signatures of hadron-quark mixed phase in gravitational waves. *Phys. Rev. D*, 83:024014, Jan 2011.
- [91] Kip S. Thorne and Alfonso Campolattaro. Non-Radial Pulsation of General-Relativistic Stellar Models. I. Analytic Analysis for $L \geq 2$. *Astrophysical Journal*, vol. 149, p.591, September 1967.
- [92] Tianqi Zhao, Constantinos Constantinou, Prashanth Jaikumar, and Madappa Prakash. Quasinormal g modes of neutron stars with quarks. *Phys. Rev. D*, 105:103025, May 2022.
- [93] N. Andersson and K. D. Kokkotas. Towards gravitational wave asteroseismology. *Monthly Notices of the Royal Astronomical Society*, 299(4):1059–1068, October 1998.
- [94] Antonino Del Popolo, Morgan Le Delliou, and Maksym Deliyergiyev. Neutron Stars and Dark Matter. *Universe*, 6(12):222, November 2020.
- [95] Cédric Jockel and Laura Sagunski. Fermion Proca Stars: Vector-Dark-Matter-Admixed Neutron Stars. *Particles*, 7(1):52–79, January 2024.
- [96] Cédric Jockel. Scalar- and Vector Dark Matter Admixed Neutron Stars. *arXiv e-prints*, page arXiv:2308.12174, August 2023.